Title

Vacancy coalescence during oxidation of iron nanoparticles

Authors

Cabot, Andreu
Puntes, Victor F.
Shevchenko, Elena
et al.

Publication Date

2007-06-23

Vacancy Coalescence during Oxidation of Iron Nanoparticles

Andreu Cabot,[†] Victor F. Puntes,[‡] Elena Shevchenko,[§] Yadong Yin,[§,‖] Lluís Balcells,[⊥]
Matthew A. Marcus,[¶] Steven M. Hughes,[#] and A. Paul Alivisatos*[,†,§,#]

Materials Sciences Division, Molecular Foundry, and Advanced Light Source, Lawrence Berkeley National Laboratory, Berkeley, California 94720, Institut Català d' Estudis i Recerca Avançat and Institut Catalá de Nanotecnologia, Bellaterra 08193, Barcelona, Spain, Institut de Ciència de Materials de Barcelona, (ICMAB-CSIC), Campus UAB, Bellaterra 08193, Spain, and Department of Chemistry, University of California at Berkeley, Berkeley, California 94720

E-mail: alivis@berkeley.edu

Iron oxide nanoparticles are widely studied because they occur naturally, they are readily synthesized artificially, and they have interesting chemical and magnetic properties as well as applications in in vivo magnetic imaging. One of the most established approaches to producing such particles is to first prepare elemental iron nanoparticles and subsequently oxidize them. A wide range of morphologies and compositions have been observed when iron nanoparticles are oxidized, ranging from iron/iron oxide core−shell structures[1] to iron/iron oxide core−void−shell structures,[2] iron oxide solid spheres,[3,4] or even iron-based hollow structures.[2,5] There is still no clear picture of the diffusion processes that accompany the chemical transformations from an elemental nanoparticle of iron to the corresponding oxides. Here we demonstrate that there is a large intermediate temperature regime ($T < 250$ °C), in which hollow iron oxide nanoparticles of 4−11 nm are spontaneously formed during iron nanoparticle oxidation in solution, due to the nanoscale Kirkendall effect. These observations can help to systematize our understanding of the temperature dependence of the inward and outward diffusion processes in iron nanoparticle oxidation, enabling improved morphology and composition control.

Iron nanoparticles can be obtained by decomposition of iron pentacarbonyl in organic solvents containing amines.[2] In order to prepare iron nanoparticles, 0.4 mL of $Fe(CO)_5$ was injected at 200 °C into 10 mL of air-free octadecene ($C_{18}H_{38}$) containing 0.67 mmol of oleylamine under vigorous stirring. The resulting solution was reacted for 20 min. By changing the reaction parameters, the particle size could be effectively tuned (Supporting Information, SI). As synthesized, iron nanoparticles are quasi-amorphous, as indicated by X-ray diffraction (XRD) analysis. X-ray absorption spectroscopy (XAS) studies identify iron as their main component. A shift of the spectrum to lower energies points toward the presence of some carbon in the iron particles (SI).[6]

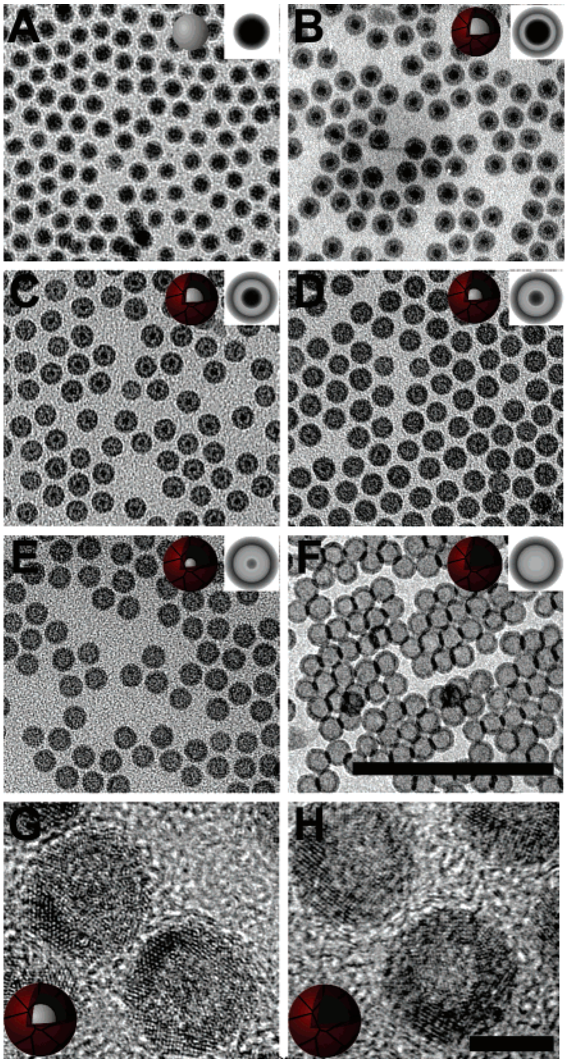

Figure 1. TEM micrographs of iron/iron oxide nanoparticles exposed to dry 20% oxygen: (A) <1 min at room temperature; (B) 1 h at 80 °C; (C) 12 h at 80 °C; (D) 5 min at 150 °C; (E) 1 h at 150 °C; (F) 1 h at 350 °C on a substrate; (G,H) high-resolution of partial and full oxidized iron nanoparticles. Low- and high-resolution scale bars correspond to 100 and 6 nm, respectively. Two-dimensional projections of the cross sections for electron scattering in iron/iron(III) oxide core−void−shell nanospheres are shown as insets. The simulated evolution of the particle size, core diameter, and shell thickness corresponds to an oxide growth at the oxide/solution interface.

In order to oxidize iron nanoparticles, we flow a dry 20% oxygen mixture in argon through the colloidal solution (20 mL/min). Figure 1 shows the conversion of iron into iron oxide nanoparticles under a range of temperatures and times. The formation of a first thin oxide layer on the iron surface is very rapid, even at room temperature. Iron nanoparticles processed in air-free conditions, but exposed to the atmosphere only during rapid transfer to a grid and introduction into a transmission electron microscope (TEM), already show a thin oxide shell (Figure 1A). The subsequent oxide formation is substantially slower; estimations based on the Cabrera−Mott and Fromhold−Cook models[7] have shown that the growth of 4 nm thick oxide layers in iron films can take ∼600 years at room

---

[†] Materials Science Division, Lawrence Berkeley National Laboratory.
[‡] Institut Català d' Estudis i Recerca Avançat & Institut Catalá de Nanotecnologia.
[§] Molecular Foundry, Lawrence Berkeley National Laboratory.
[⊥] Institut de Ciència de Materials de Barcelona.
[¶] Advanced Light Source, Lawrence Berkeley National Laboratory.
[#] University of California at Berkeley.
[‖] Current address: Department of Chemistry, University of California at Riverside, Riverside, CA 92521. E-mail: yadong.yin@ucr.edu.

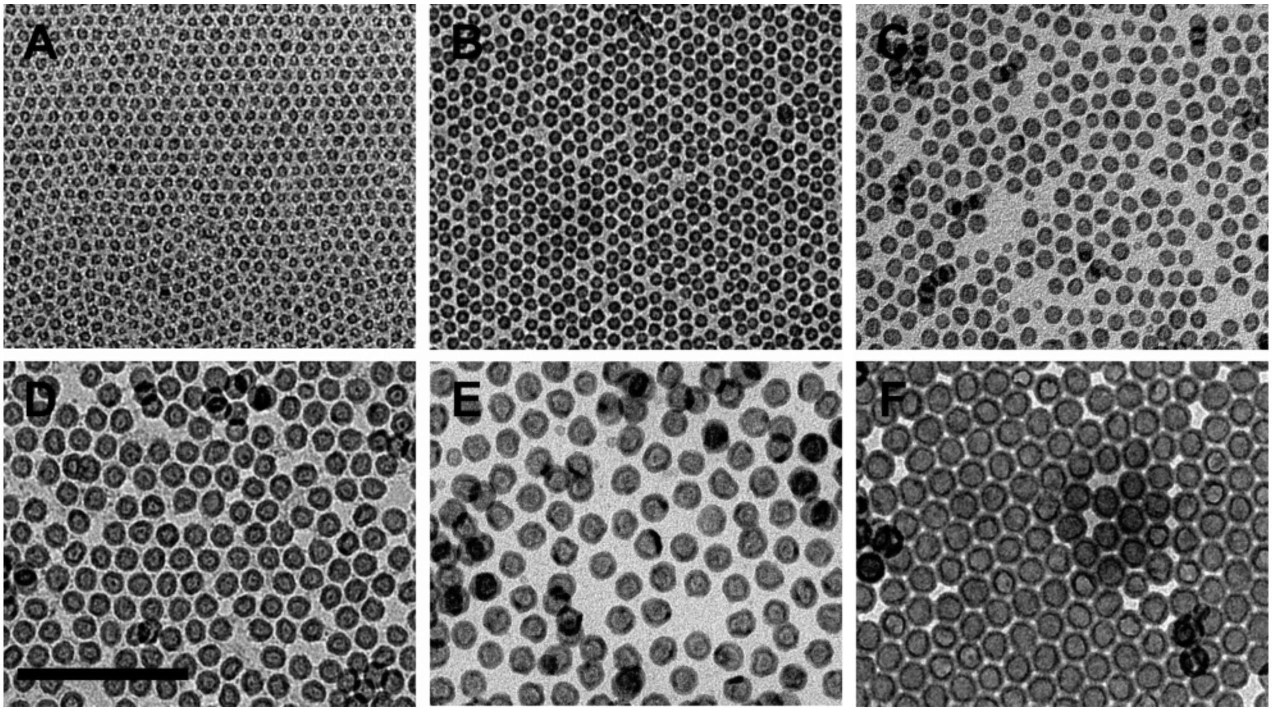

Figure 2. TEM micrographs of iron nanoparticles with different sizes oxidized at 250 °C in solution (A−E), and at 350 °C while supported on a substrate (F). Scale bar corresponds to 100 nm.

temperature.[8] This process can be accelerated by taking advantage of the exponential temperature dependence of the iron diffusivities. As a result, the reaction temperature and oxidation time allow to precisely tune the thickness of an initial oxide shell. The second stage of the oxidation process can be seen clearly in Figure 1B−F. Of particular interest here is the clear observation, even at very early stages, of a very thin low-density region between the initial iron particle and the outer oxide layer. This is due to the coalescence of voids at the interface and is a clear signature of iron diffusing outward through the initial oxide shell, leaving vacancies behind, in the nanoscale Kirkendall effect.[9,10] TEM micrographs of the partially oxidized particles show three differentiated contrast regions (Figure 1). The darker inner region corresponds to the iron core. The outermost shell, corresponding to a lower-density material, is the iron oxide. As the chemical transformation proceeds, the oxide shell grows thicker due to the continual appearance and subsequent oxidation of iron atoms on the outermost surface of the oxide. The disappearance of the spherical iron core in the center of the hollow particle can be clearly observed. When iron atoms diffuse outward, the vacancies left behind ultimately coalesce into a single central void (Figure 1F). These results are consistent with a previous study on the room-temperature oxidation of iron clusters supported on carbon grids.[8] The nanoscale Kirkendall effect was initially described for reactions of Co nanoparticles with oxygen, sulfur, and selenium.[10] Careful TEM investigation of cobalt nanoparticles oxidized with selenium revealed thin filamentous connections between the shell and the central metal particle. These metal bridges provide a fast transport path for diffusion of metal atoms from the core to the oxide shell.

It is interesting to consider the range of behaviors which can be expected from this system as a function of the temperature and the nanocrystal size. Dissociative adsorption of oxygen, followed by place-exchange with the surface iron is considered the first step in the oxidation of iron surfaces.[11] Once an initial oxide layer is formed, electron transport from the metal core to the adsorbed oxygen through the oxide layer allows oxidation to carry on. The contact potential of the chemisorbed oxygen results in a strong electric field able to drive the ion diffusion.[7,11,12] At temperatures below 150 °C, the dominant electron transport mechanism is by tunneling through the thin oxide layer. Electron tunneling is operative only up to a thickness of ∼1−3 nm.[11,12] Above this temperature, an additional electron supply is provided by thermoemission of electrons from the iron into the oxide conduction band.[12] This additional source of electrons allows the oxide growth to proceed further, up to ∼10 nm thick oxide layers.

The location of the iron−oxygen reaction front is determined by the relative diffusion rates of iron and oxygen ions, as well as the shell thickness, microstructure, and temperature. Our experimental results show the coalescence of vacancies at the metal/oxide interface, which points toward an initial net outward material flow. This observation is consistent with faster outward diffusion of iron cations than inward flow of oxygen anions.[8] The oxide growth strongly slows down for shells thicker than ∼2.0 ± 0.4 nm at temperatures lower or equal to 250 °C. In this temperature range, only iron particles smaller than ∼8 nm could be completely converted into hollow oxide particles. The oxidation rate of larger particles becomes imperceptible for ∼3 ± 0.4 nm thick shells, trapping a core inside the oxide shell (Figure 2B−E).

When heating the particles in solution at a higher temperature (T ∼ 250−300 °C), cracks are formed on the oxide shells (SI). The growth of the crystal domains creates large stresses that lead to the shell fragmentation. The temperature range at which cracks are formed depends on the shell thickness and thus on the particle size. In large iron nanoparticles, the shell brakes before the oxidation of the whole particle is complete. The shell fragmentation allows the solvent and oxygen to reach and oxidize the core. No such cracks are observed upon heating of the same particles on a substrate in the absence of a solvent. In this way, the oxidation of iron nanoparticles at 350 °C leads to the formation of hollow iron oxide nanoparticles with diameters as large as 20 nm, and ∼4−5 nm thick shells (Figure 2F).

The formation of hollow iron oxide nanoparticles under the TEM electron beam when analyzing Fe nanoparticles stabilized by trioctylphosphine oxide has been reported.[4] To exclude such an effect on our particles during TEM characterization, the particles at different oxidation stages were kept under the electron beam during periods of more than 30 min. No electron-beam-induced changes were observed in any of the amine-stabilized particles we analyzed (SI).

As indicated by high-resolution TEM (HRTEM), the oxide shells around the colloidal Fe particles are polycrystalline (Figure 1F). Crystal domains extend across the entire shell. However, no preferential orientation of the lattices across the shell could be deduced from our data. Regarding the crystal structure, while XRD data allows us to safely exclude the presence of the hematite (α-Fe_2O_3) phase, the line broadening associated with the small crystal size domains makes it impossible to distinguish between magnetite (Fe_3O_4) and maghemite (γ-Fe_2O_3) phases. Nonetheless, the X-ray absorption near edge structure (XANES) spectra of the particles oxidized in the temperature range between 200 and 250 °C resemble that of a maghemite reference sample (SI). Oxidized nanoparticles show no band at the pre-edge corresponding to Fe^{2+} and a shift of the absorption spectrum to higher energies than that obtained for magnetite.[13] Both features allow us to identify the iron oxide phase of the completely oxidized particles as maghemite. Further, maghemite is a semiconductor with a 2.03 eV band gap, while magnetite is a semimetal with a 0.14 eV band gap. Optical spectra of hollow nanoparticles show the absorption band at wavelengths lower than $\sim$600 nm, consistent with the maghemite phase of the fully oxidized iron nanoparticles (SI).

While our experimental results point toward the formation of maghemite by oxidation of the iron nanoparticles at temperatures in the range of 200−250 °C, other authors report the total or partial formation of magnetite by oxidation of iron at lower temperatures or using other oxygen precursors.[2,13,14] Maghemite and magnetite are both thermodynamically metastable phases. However, the preeminence of the maghemite phase over magnetite is consistent with kinetic considerations: while the small kinetic barrier for the transformation of magnetite to maghemite allows this phase transition to take place at low temperatures, the maghemite to hematite transformation is inhibited at temperatures lower than 300−400 °C because of the very different crystal structures.[13,15] The slight difference between magnetite and maghemite crystalline lattices might explain their strong dependence on the oxidation conditions. The presence of water has also an important influence on the oxidation procedure and the final nanostructures obtained.[16]

In summary, we detailed a synthetic route, based on the nanoscale Kirkendall effect, to produce colloidal solutions of monodisperse iron/iron oxide core−void−shell nanostructures and hollow maghemite nanoparticles with controllable particle size and shell thickness. A limitation on the size of the hollow nanostructures that can be synthesized in solution exists. This depends on the iron diffusivities and the growth of the crystal size domains in the polycrystalline oxide shells.

Acknowledgment. This work was supported by the Director, Office of Science, Office of Basic Energy Sciences, Materials Sciences and Engineering Division, of the U.S. Department of Energy under Contract No. DE-AC02-05CH11231 and by the DARPA/AFOSR DURINT Program Grant No. F49620-01-1-0474. A.C. thanks the Generalitat de Catalunya, Departament d'Universitats, Recerca i Societat de l'Informació for financial support. V.F.P. thanks financial support from MAT2006-13572-C02-02. We thank Prof. J. Long and his group for the assistance and use of their SQUID.

Supporting Information Available: Detailed synthesis and experimental procedures, UV−vis, XRD, and XAS of the iron/iron oxide nanoparticles, SQUID of the final iron oxide shells, histograms of the particle sizes, and analysis of the electron beam influence during TEM imaging and of the high-temperature oxidation of the particles in solution. This material is available free of charge via the Internet at http://pubs.acs.org.

References

(1) Carpenter, E. E.; Calvin, S.; Stroud, R. M.; Harris, V. G. *Chem. Mater.* **2003**, *15*, 3245−3246.

(2) (a) Peng, S.; Wang, C.; Xie, J.; Sun, S. *J. Am. Chem. Soc.* **2006**, *128*, 10676−10677. (b) Peng, S.; Sun, S. *Angew. Chem., Int. Ed.* **2007**, *46*, 1−5.

(3) Hyeon, T.; Lee, S. S.; Park, J.; Chung, Y.; Na, H. B. *J. Am. Chem. Soc.* **2001**, *123*, 12798−12801.

(4) Latham, A. H.; Wilson, M. J.; Schiffer, P.; Williams, M. E. *J. Am. Chem. Soc.* **2006**, *128*, 12632−12633.

(5) Farrell, D.; Majetich, S. A.; Wilcoxon, J. P. *J. Phys. Chem. B* **2007**, *107*, 11022−11030.

(6) van Wonterghem, J.; Mørup, S.; Charles, S. W.; Wells, S.; Villadsen, J. *Phys. Rev. Lett.* **1985**, *55*, 410−412.

(7) (a) Fromhold, A. T., Jr.; Cook, E. L. *Phys. Rev.* **1967**, *158*, 600−612. (b) Fromhold, A. T., Jr.; Cook, E. L. *Phys. Rev.* **1967**, *163*, 650−664. (c) Cabrera, N.; Mott, N. F. *Rep. Prog. Phys.* **1949**, *12*, 163−184.

(8) Wang, C. M.; Baer, D. R.; Thomas, L. E.; Amonette, J. E.; Antony, J.; Qiang, Y.; Duscher, G. *J. Appl. Phys.* **2005**, *98*, 094308.

(9) Smigelskas, A. D.; Kirkendall, E. O. *Trans. AIME* **1947**, *171*, 130−142.

(10) (a) Yin, Y.; Rioux, R. M.; Erdonmez, C. K.; Hughes, S.; Somorjai, G. A.; Alivisatos, A. P. *Science* **2004**, *304*, 711−714. (b) Yin, Y.; Erdonmez, C. K.; Cabot, A.; Hughes, S.; Alivisatos, A. P. *Adv. Funct. Mater.* **2006**, *16*, 1389−1399.

(11) (a) Grosvenor, A. P.; Kobe, B. A.; McIntyre, N. S. *Surf. Sci.* **2004**, *565*, 151−162. (b) Grosvenor, A. P.; Kobe, B. A.; McIntyre, N. S. *Surf. Sci.* **2005**, *574*, 317−321.

(12) (a) Leibbrandt, G. W. R.; Hoogers, G.; Habraken, F. H. P. M. *Phys. Rev. Lett.* **1992**, *68*, 1947−1950. (b) Graat, P. C. J.; Somers, M. A. J.; Vredenberg, A. M.; Mittemeijer, E. J. *J. Appl. Phys.* **1997**, *82*, 1416−1422. (c) Roosendaal, S. J.; Vredenberg, A. M.; Habraken, F. H. P. M. *Phys. Rev. Lett.* **2000**, *84*, 3366−3369.

(13) Signorini, L.; Pasquini, L.; Savini, L.; Carboni, R.; Boscherini, F.; Bonetti, E.; Giglia, A.; Pedio, M.; Mahne, N.; Nannarone, S. *Phys. Rev. B* **2003**, *68*, 195423.

(14) Leibbrandt, G. W. R.; Spiekman, L. H.; Habraken, F. H. P. M. *Surf. Sci.* **1993**, *287/288*, 250−254.

(15) (a) Schimanke, G.; Martin, M. *Solid State Ionics* **2000**, *136−137*, 1235−1240. (b) Ayyub, P.; Multani, M.; Barma, M.; Palkar, V. R.; Vijayaraghavan, R. *J. Phys. C: Solid State Phys.* **1988**, *21*, 2229−2245.

(16) (a) Grosvenor, A. P.; Kobe, B. A.; McIntyre, N. S. *Surf. Sci.* **2004**, *572*, 217−227. (b) Roosendaal, S. J.; Bakker, J. P. R.; Vredenberg, A. M.; Habraken, F. H. P. M. *Surf. Sci.* **2001**, *494*, 197−205.